Heliyon 9 (2023) e12710

Contents lists available at ScienceDirect

Heliyon

journal homepage: www.cell.com/heliyon

Research article

A crossed-polarized four port MIMO antenna for UWB communication

Adamu Halilu Jabire [a,f], Salisu Sani [b], Sani Saminu [c,d], Mohammed Jajere Adamu [e], Mousa I. Hussein [f,*]

[a] Department of Electrical and Electronics Engineering, Taraba State University, Jalingo, Nigeria
[b] Department of Electrical Engineering, Ahmadu Bello University, Zaria, Kaduna State, Nigeria
[c] Department of Biomedical Engineering, University of Ilorin, Ilorin, Nigeria
[d] State Key Laboratory of Reliability and Intelligence of Electrical Equipment, Hebei University of Technology, Tianjin 300130, China
[e] School of Microelectronics, Tianjin University, Tianjin, China
[f] Department of Electrical and Communication Engineering, UAE University, Al Ain, United Arab Emirates

ARTICLE INFO

Keywords:
UWB-MIMO
Metamaterials
Mutual coupling
Cross-polarized elements
Correlation coefficient

ABSTRACT

This paper presents a compact, crossed-polarized, ultra-wideband (UWB) four-ports multiple-input-multiple-output (MIMO) printed antenna. The proposed antenna is constructed from four microstrip circular patch elements fed by a 50-Ω microstrip line. Two metamaterial cell elements, in the form of a rectangular concentric double split ring resonator (SRR), are placed at the upper plane of the substrates for bandwidth improvement and isolation enhancement. The ultra-wideband frequency response is achieved using a defective ground plane. Surface current flow between the antenna's four elements is limited to ensure maximum isolation. The four-port MIMO system is designed with orthogonal antenna elements orientation on an FR4 substrate with a loss tangent of 0.02 and an overall size of 30 mm × 30 mm × 1.6 mm. Such orientation resulted in less than −17dB port-to-port isolation and an impedance bandwidth of 148% (3.1–12 GHz). The proposed UWB-MIMO antenna achieved a maximum realized gain of 6.2dBi with an efficiency of 87%. The measured and simulated results are in good agreement over the operating frequency band (3.1–12 GHz). The results also provide overall good diversity performance with the TARC < −10 dB, ECC < 0.001, DG > 9.9, MEG < −3 dB and CCL <0.1. The proposed antenna is well-suited for applications in WLAN, WIMAX and GPRs.

1. Introduction

The need and requirement for data throughput without interference are in high demand nowadays. With multiple-input-multiple-output (MIMO) technology, a radio link can have a greater capacity by employing multiple transmit and receive antennas to achieve multipath propagation [1]. MIMO system increases communication channel capacity, network reliability, and data speed in a wide range of wireless networks by harnessing the full capabilities of wireless communication systems. Antenna deployment close to each other is necessary to meet the characteristics mentioned above. According to the federal communication commission (FCC), ultra-wideband applications use frequencies between 3.1 and 10.6 GHz [1]. However, the UWB system has some advantages, such as

* Corresponding author.
E-mail address: mihussein@uaeu.ac.ae (M.I. Hussein).

https://doi.org/10.1016/j.heliyon.2022.e12710
Received 2 July 2022; Received in revised form 19 November 2022; Accepted 21 December 2022
Available online 29 December 2022

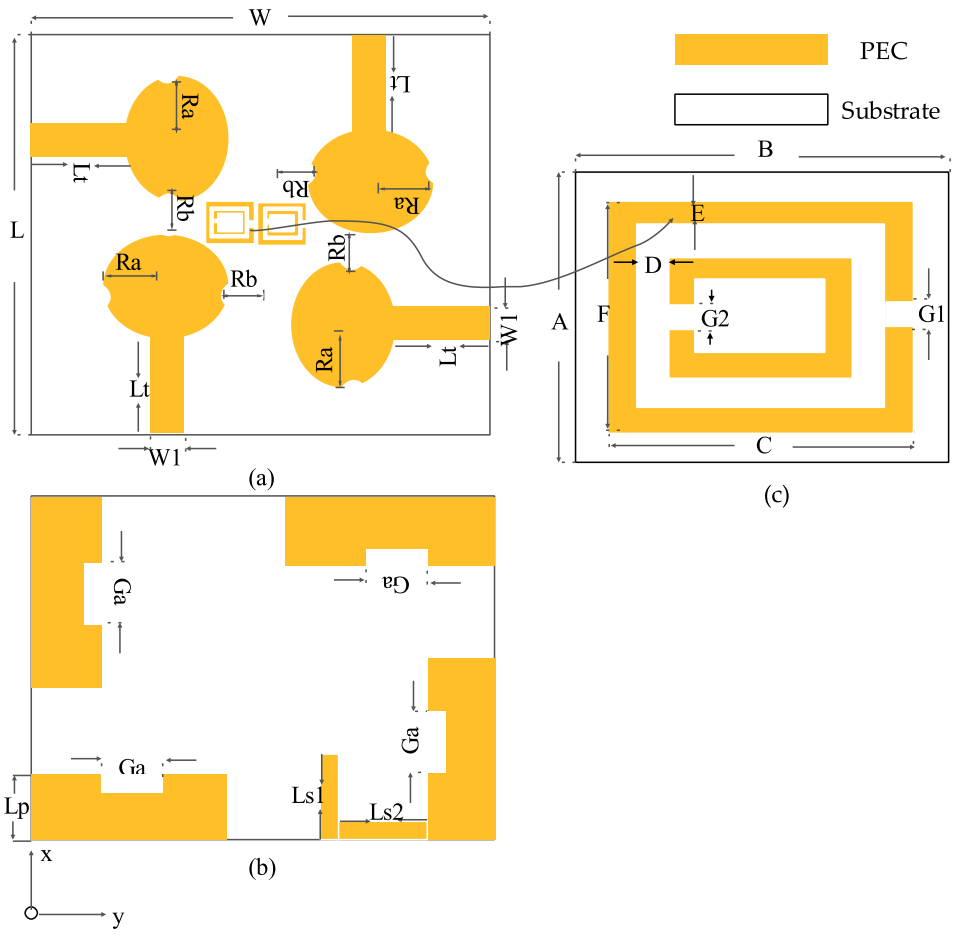

Fig. 1. UWB-MIMO antenna geometry, (a) top view, (b) bottom view, (c) unit cell.

low power consumption, high data rates, and a simple hardware design. The MIMO antenna system can reduce the fading caused by multipath fading, which is always a problem with UWB technology. Therefore, combining UWB technology with MIMO will improve system performance. For both mobile terminals and base stations, compact MIMO antennas are required due to limited space and aesthetic reasons. The proximity of antenna elements leads to mutual coupling between them. Today, we live in the era of 5G, which demands high-speed data transmission, low latency, and high reliability. As a result of radiations from free space, surface currents, and surface waves, there is a phenomenon called mutual coupling that degrades the signal-to-noise ratio (SNR) and convergence of an adaptive array [2–7].

With an array of signal processing techniques that degrade carrier frequency offset (CFO), channel estimation, and angle of arrival estimation, the total active reflection coefficient of a MIMO antenna may be impacted. In mutual coupling, communication on adjacent channels may be hampered by significant out-of-band (OOB) emissions from power amplifiers (PAs). The mutual coupling has been decreased in the digital arena by enhancing MIMO precoding and decoding algorithms [8]. Before calculating the weight vector of adaptive algorithms, the received voltages are modified to remove mutual coupling. The signal-to-interference noise ratio (SINR) can be increased by decreasing the relative interference or noise during post-processing. It is not necessary to correct electromagnetic interactions to preserve SINR. The electromagnetic suppression in the digital domain can be improved to some extent using the above method. An efficient decoupling method is more effective at mitigating mutual coupling effects from the antenna's perspective. As a result, antenna-based decoupling techniques must be developed [9].

Decoupling is accomplished using different methods. Defected ground structures [10], decoupling networks [11], electromagnetic band gap structures (EBG) [12], neutralizing lines [13], parasitic or slot elements [14] and complementary split-ring resonator (CSRR) [15] are an example of such decoupling techniques. A UWB-MIMO antenna with dual ports is described in Ref. [16]; it exhibits wideband characteristics with a frequency range of 3.0–11.0 GHz and four rejection bands. In Ref. [17], slots of inverted L and U shapes are reported to provide quadruple notch characteristics at 3.3 GHz, 4.03 GHz and 5.4 GHz. Additionally, the antenna offers isolation of −25 dB. A flexible CPW-fed MIMO antenna is presented in Ref. [18]; to achieve good polarization diversity, a high impedance width of 125.83%, a maximum gain of 6.8 dBi, and an efficiency of 89%, four identical elements are arranged symmetrically in a successive rotational manner. The authors in Ref. [19] miniaturized a UWB-MIMO antenna by sharing rhombic slot

Table 1
Optimal parameters and size of the antenna.

Parameter	Size (mm)	Parameter	Size (mm)	Parameter	Size (mm)
A	7	G_1	0.35	L_{s1}	10
B	7	G_2	0.35	L_{s2}	8
C	5	G_a	3	R_a	9.35
D	3	L	30	R_b	1
E	0.4	L_t	11.05	W	30
F	5	L_p	10	W_1	2.5

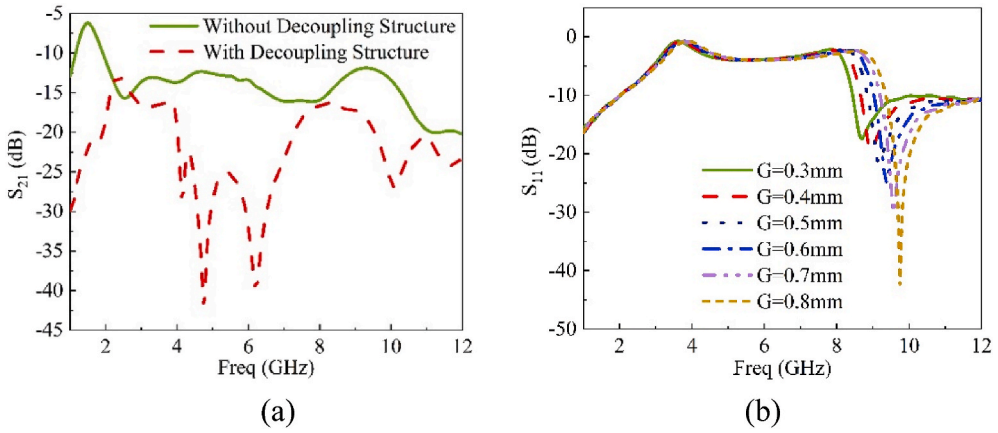

Fig. 2. S_{21} with & without decoupling metamaterial structure (a), different gap capacitance (b).

radiation with four microstrip feeders. The notched characteristics are realized by opening C-slots and L-slots and adding an H-shaped EBG structure. The antenna has a good diversity performance, high isolation of −40 dB, peak gain of 5.5 dBi and radiation efficiency of 75%–90%. A letter in Ref. [20] demonstrated a quasi U-shape patch on the upper plane and a stepped slot in the ground plane for wideband impedance match and dual-band notch capability. The utilization of defective ground structure for an elliptical planar antenna has been studied in Ref. [21], where the DGS is employed to realize a UWB frequency response. The work in Ref. [22] used two symmetrical half-slot elements with CPW-fed structures, and a Y-shaped slot separated at the bottom center of the common ground. The slots efficiently prevent the current flow at low UWB frequency and reduce the mutual coupling between the MIMO elements. A novel four-element MIMO antenna for UWB applications is reported in Ref. [23]; the antenna is CPW-fed and consists of four orthogonal parts. Based on the proposed antenna, an impedance width from 2.1 to 20 GHz is achieved with notch frequencies of 3.3 GHz–4.1 GHz and 8.2 GHz–8.6 GHz. Notches achieved can filter out interference from WiMAX and radar applications [24] discusses the use of neutralization line technique for the design of MIMO antennas for UWB communications. Measured bandwidths were 95.22% (3.51–9.51 GHz) and 96.47% (3.52–10.0 GHz), with better isolation of −23 dB. The MIMO antenna provides a peak gain of 2.91 dBi and has better diversity metrics. Moreover, the antenna design presented in Ref. [25] is a very small-sized 2-element planar antenna. The UWB response is obtained using a rectangular stepped slot and a z-shaped slot etched in the ground plane. The geometrical size of the reported structure is 23 × 26 × 0.8 mm^3, and the antenna has a peak gain of 5 dBi with an efficiency of 80%.

UWB-MIMO antennas are expected to have high isolation, low mutual coupling, low correlation, and low total active reflection coefficients. It will enhance the wide throughput bandwidth. This paper developed a 4-port UWB-MIMO antenna to obtain a wide impedance bandwidth of 3.1–12 GHz and ensure that the MIMO elements would have low mutual interaction. To achieve a minimal isolation level of −17 dB, a split rectangular loop resonator (SRLR) is used. In summary, the advantage of our proposed UWB-MIMO antenna is its simple design for MIMO application, UWB operation from 3.1 to 12 GHz, sensing applications like tumor detection, WLAN, WIMAX, GPRs, high diversity, and finally, high efficiency and gain. The proposed antenna's analysis and configuration are covered in Section 2, equivalent circuit models and the proposed antenna analysis are covered in Section 3, the experimental validation and MIMO performance are covered in Section 4, and Section 5 is the conclusion.

2. Design of UWB cross-polarized MIMO antenna

Fig. 1(a–c) shows the suggested cross-polarized 4-element MIMO antenna model. The simulations and optimization have been supported by Computer Simulation Technology (CST), with an overall size of 0.6 λ_0 × 0.6 λ_0 × 0.032 λ_0 at 6 GHz center frequency, the proposed antenna was designed utilizing the FR-4 substrate (relative permittivity of 4.3 and loss tangent of 0.02). The patch is fed by a 50-Ω microstrip line and has a circular form with etched curves. A defective ground structure that is not connected is built to aid in lowering the mutual coupling between MIMO elements.

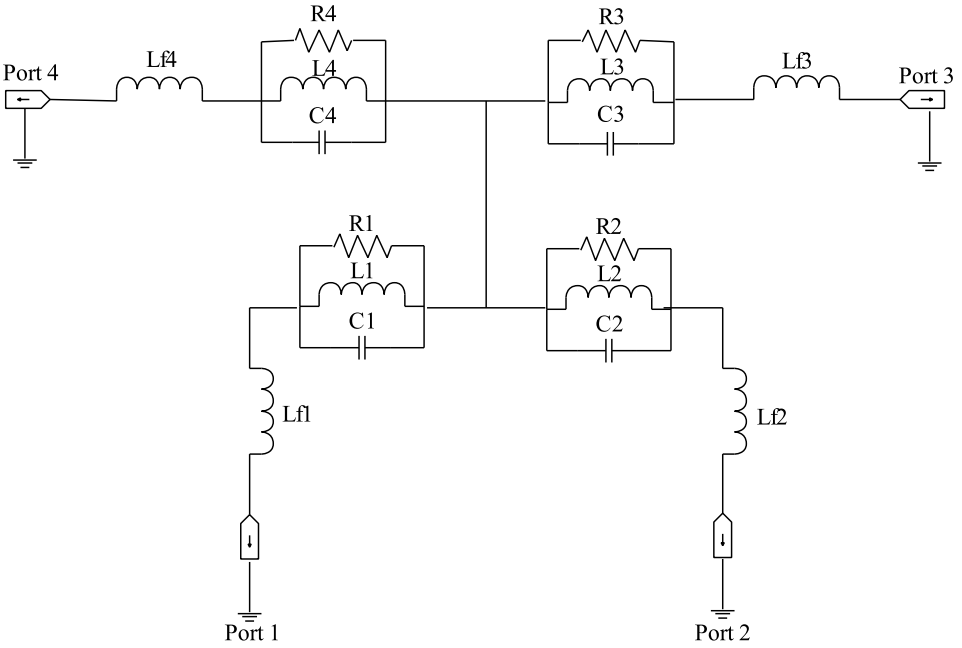

Fig. 3. Circuit model for UWB-MIMO antenna.

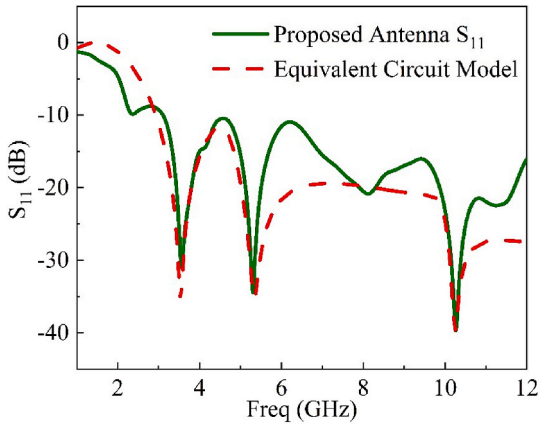

Fig. 4. Circuit model and S_{11} of UWB-MIMO.

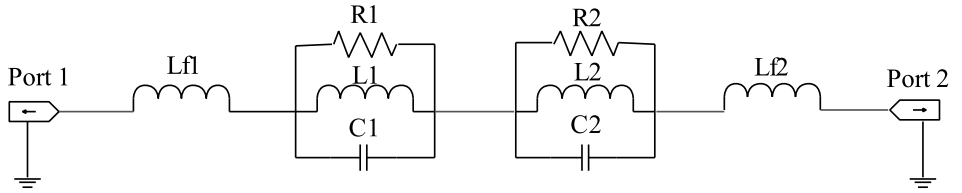

Fig. 5. Circuit model for a unit cell metamaterial.

To further improve the isolation, a split rectangular loop resonator (SRLR) is employed at the Centre of the model, which acts as a filter that upsets the flow of current and surface waves. All parameters have undergone a thorough parametric study, and Table 1 provides the best performance values.

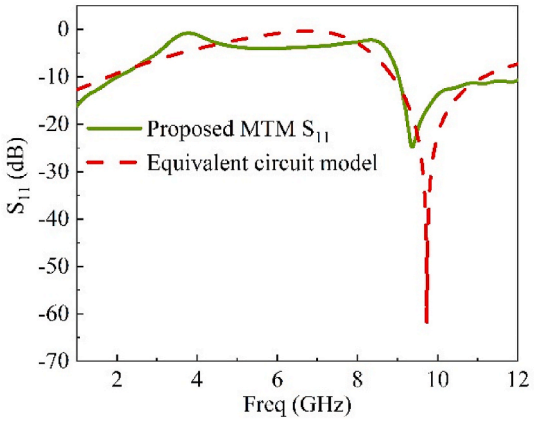

Fig. 6. Circuit model and S_{11} of a unit cell.

Table 2
Components used in UWB-MIMO circuit (R(Ω), L (nH), C(PF)).

R1 = 30266.3	R2 = 76.5	R3 = 295.7	R4 = 549.5
L1 = 10.11	L2 = 2.4	L3 = 0.213	L4 = 1.814
C1 = 1.21	C2 = 0.97	C3 = 1.22	C4 = 0.811
L_{F1} = 0.144	L_{F2} = 8.13	L_{F3} = 4.99	L_{F4} = 5.77

Table 3
The component used in a unit cell circuit model (R(Ω), L (nH), C(PF)).

R1 = 48.9	R2 = 2.73	L1 = 48.66
L2 = 1.24	C1 = 54.86	C2 = 433.1
L_f = 1.343	–	–

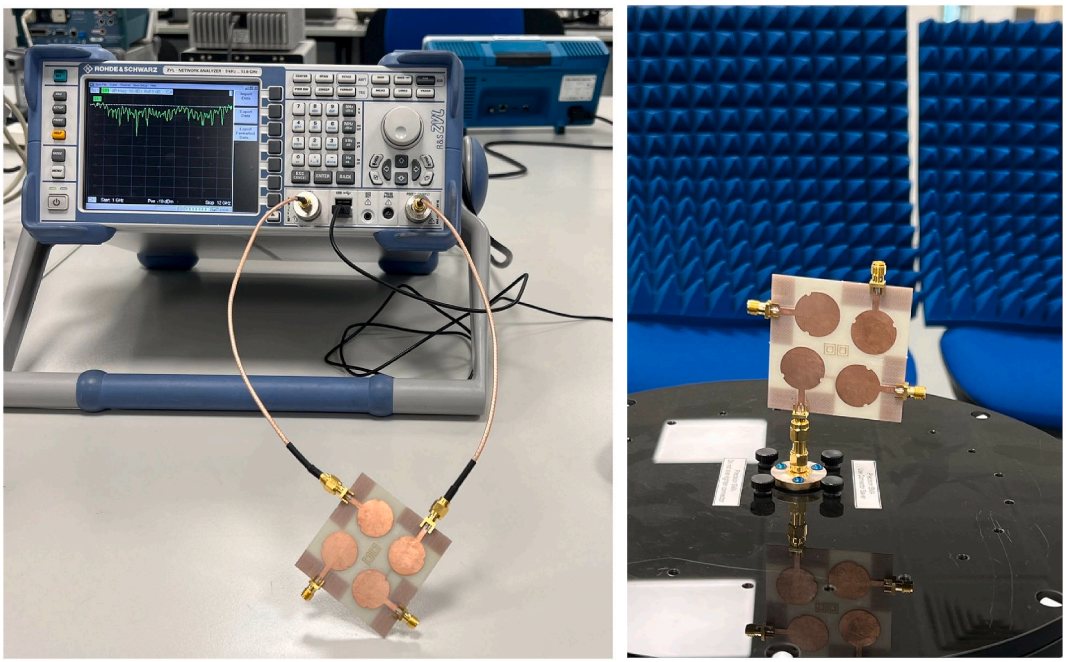

Fig. 7. Measurement set up for the proposed MIMO-UWB antenna, (a) VNA, and (b) Anechoic chamber.

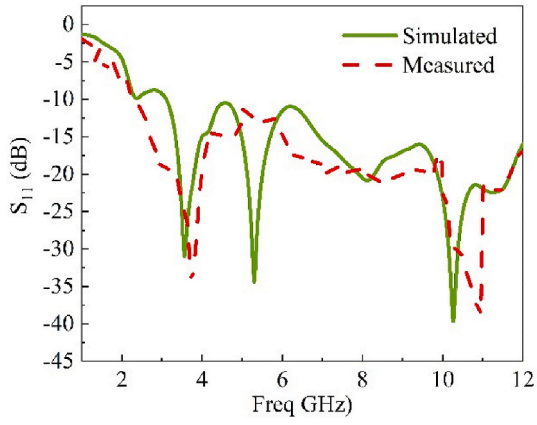

Fig. 8. Measured and simulated S_{11} of the antenna.

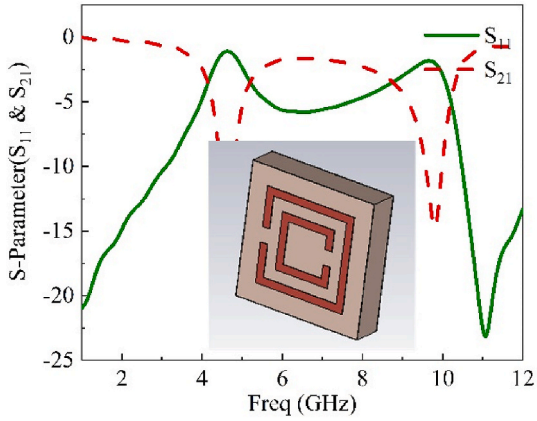

Fig. 9. S_{11} and S_{21} of the unit cell.

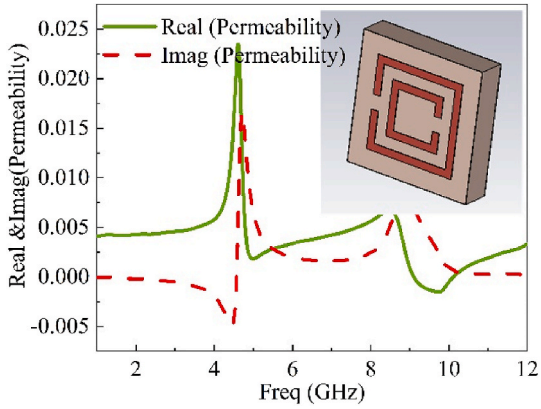

Fig. 10. Real and imaginary permeability of the unit cell.

2.1. Metamaterial parametric analysis

The parametric analysis will be based on two stages: the availability of the decoupling technique, located at the center of the model, and the cap capacitance. The effects of the decoupling structure on S21 are depicted in Fig. 2a. It is evident that the isolation has improved when the metamaterial structure is employed. Another parametric study is carried out for different gap capacitances G1 and G2. The higher the value of G, the higher the filter matching, as shown in Fig. 2b.

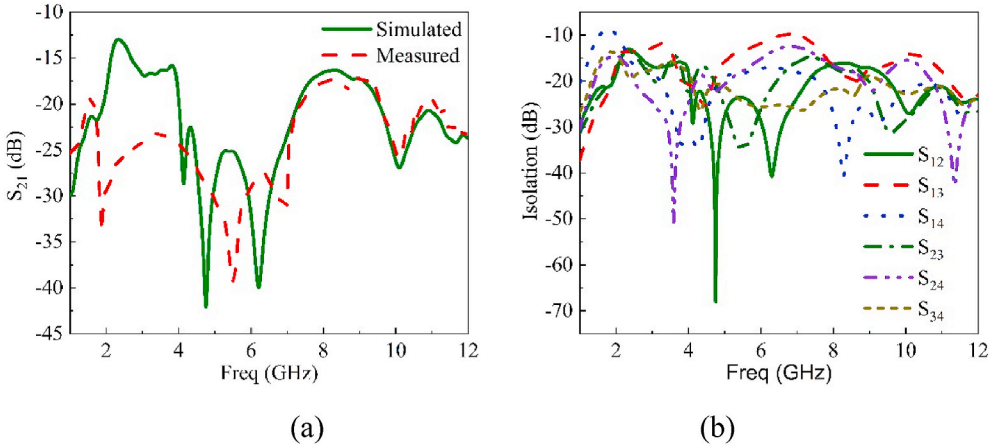

Fig. 11. Measured and simulated S_{21} (a), two ports, (b) four ports.

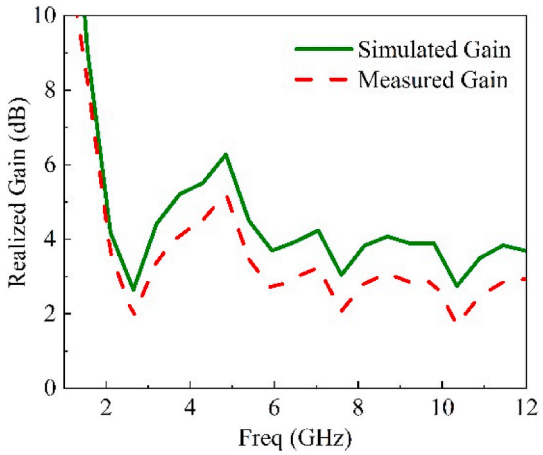

Fig. 12. Measured and simulated realized gain.

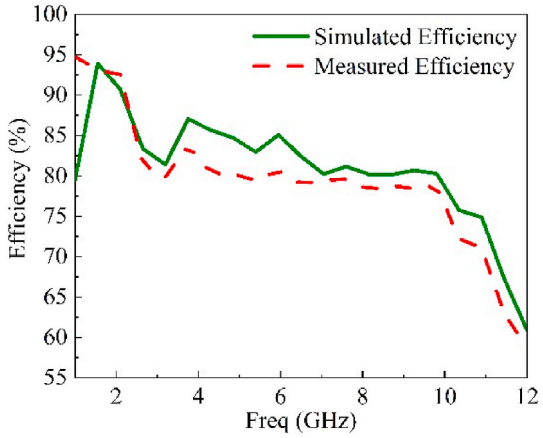

Fig. 13. Simulated and measured efficiency of the antenna.

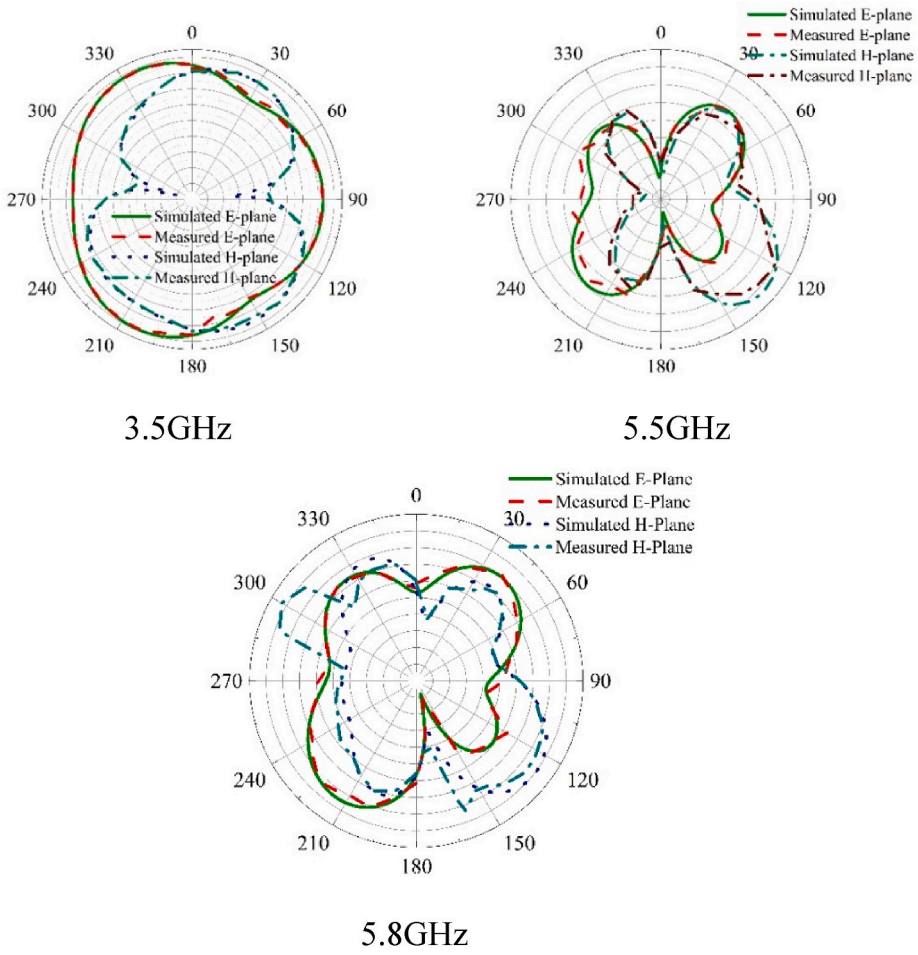

Fig. 14. Simulated and measured radiation pattern at 3.5 GHz, 5.5 GHz, and 5.8 GHz.

3. Analysis of proposed antenna and equivalent circuit

The corresponding circuit model for the proposed UWB-MIMO antenna was optimized using the ADS software, as shown in Fig. 3. The gradient optimization method is used to optimize the model parameters with each component's minimum and maximum values. Each patch and microstrip line is modeled as a combination of an inductor (L_F) and cascaded parallel RLC component [26]. Fig. 4 shows the circuit model S_{11} compared with the CST full-wave simulation. A metamaterial unit cell was also subjected to the same analysis. The resonance response is achieved after the two cascaded parallel RLC circuits. The MTM circuit model is shown in Fig. 5. The ADS $S_{11,}$ as compared with the CST model, is depicted in Fig. 6, and the optimized values of the components used are listed in Tables 2 and 3.

4. UWB-MIMO experimental results

The fabrication was carried out in a high-frequency lab at UAE University, in which the UWB-MIMO antenna was constructed on a 1.6 mm thick, double-sided FR-4 substrate. Two unit cells are integrated, having a two-square strip with a separate gap capacitance based on the periodic boundary set up in CST. The prototype is shown in Fig. 7a and b mounted on the ZVL-Network analyzer and anechoic chamber for S-parameters, far-field pattern, gain, and radiation efficiency measurements. Figs. 8–11 shows the simulated and measured results of the antenna's maximum achieved gain and efficiency. Fig. 8 displays the simulated and measured S_{11}. The scattering parameters for the unit cell metamaterial are depicted in Figs. 9 and 10 is the real and imaginary permeability curve. The antenna's isolation for both the measured and simulated is shown in Fig. 11a, using two ports, while Fig. 11b is the isolation obtained for the four ports antenna. The proposed antenna's measured and simulated realized gain is depicted in Fig. 12, with a maximum realized gain of 6.2dBi around 5 GHz. Fig. 13 displays the measured and simulated results for the antenna efficiency. The maximum value is recorded at 87%, around 4.3 GHz.

To validate the measured UWB far-field response, an anechoic chamber was used to compare the simulated results. Fig. 14 shows the measured and simulated E-plane and H-plane operating at 3.5 GHz, 5.5 GHz, and 5.8 GHz. At low frequencies, the pattern has an

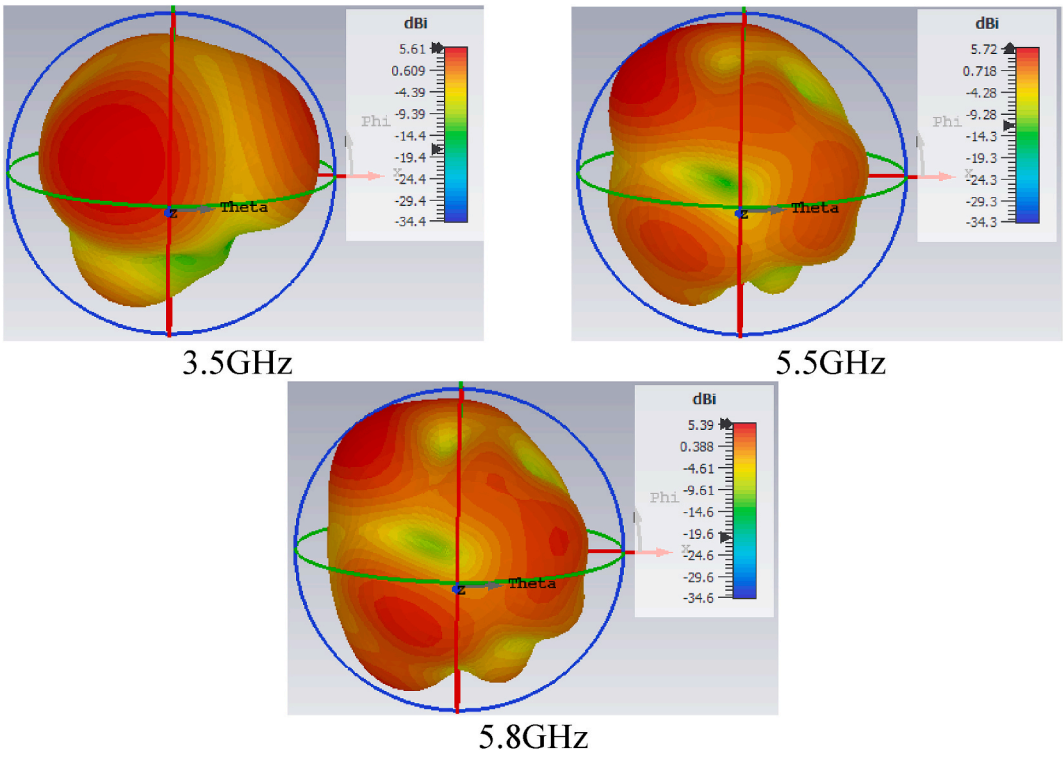

Fig. 15. 3D antenna gain at selected frequencies of 3.5 GHz, 5.5 GHz, and 5.8 GHz.

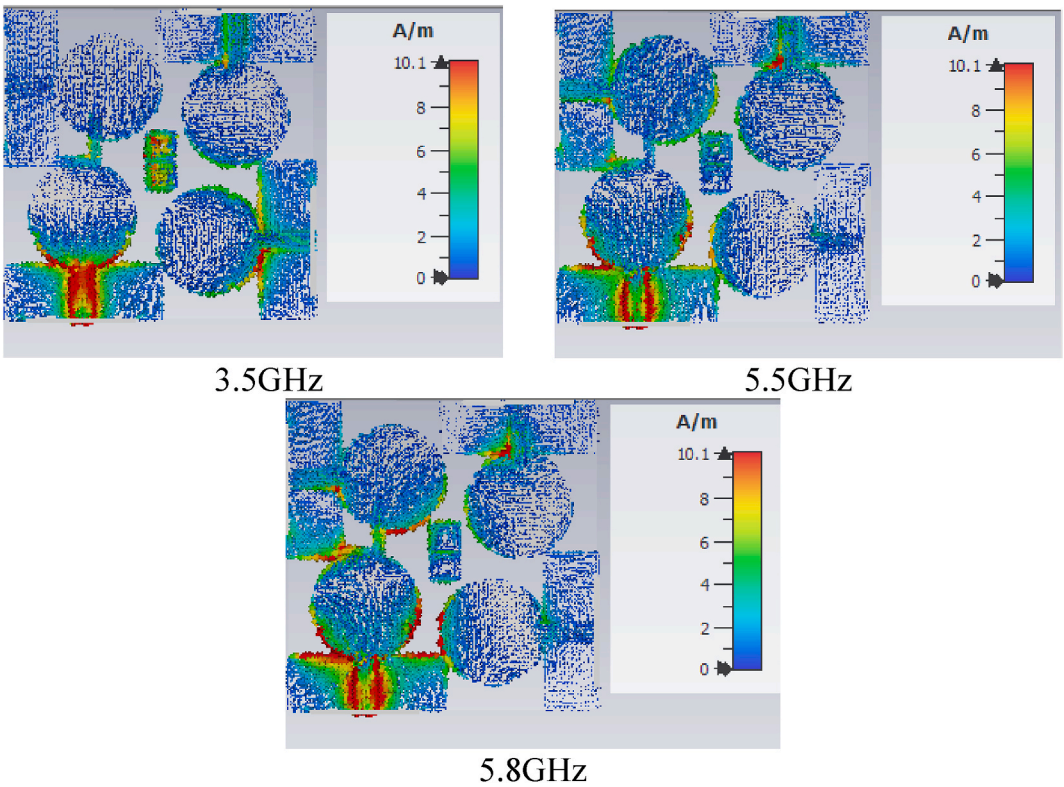

Fig. 16. Current distribution at selected frequencies of 3.5 GHz, 5.5 GHz, and 5.8 GHz when port 1 is excited.

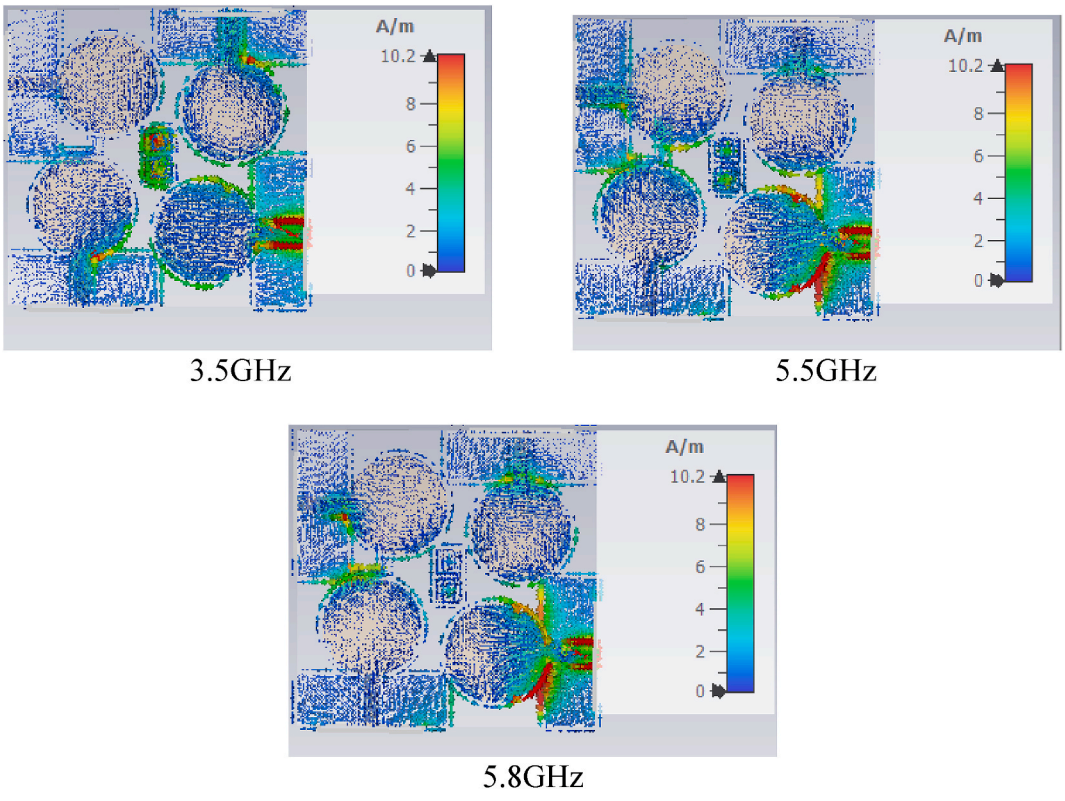

Fig. 17. Current distribution at selected frequencies of 3.5 GHz, 5.5 GHz, and 5.8 GHz when port 2 is excited.

omnidirectional layout, but as the frequency increases, the omnidirectional configuration starts to degrade. The polar antenna gains at 3.5 GHz, 5.5 GHz, and 5.8 GHz are shown in Fig. 15. As can be seen, every selected frequency has a different gain. When ports 1, 2, and 3 are excited, Figs. 16–19 displays the surface current density at 3.5 GHz, 5.5 GHz, and 5.8 GHz, respectively. An exciting port has a higher concentration of current.

Some diversity characteristics, such as the correlation coefficient (ECC), total active reflection coefficient (TARC), diversity gain (DG), mean effective gain (MEG), and channel capacity loss, have an impact on the MIMO antenna's acceptable performance. A MATLAB program was developed to obtain these parameters and confirm the measured results.

4.1. Correlation coefficient and diversity gain

The ECC measures the correlation between the nth and mth radiating elements' far-field patterns in a particular MIMO system. The ECC can be calculated using the far-field patterns [27], which are provided by Eq. (1):

$$\rho e = \frac{\left| \iint_{4\pi} \left[\vec{F}_1(\theta,\varphi) \times \vec{F}_2(\theta,\varphi) d\Omega \right] \right|^2}{\left| \iint_{4\pi} \left[\vec{F}_1(\theta,\varphi) \right] \right|^2 d\Omega \left| \iint_{4\pi} \left[\vec{F}_2(\theta,\varphi) \right] \right|^2 d\Omega} \tag{1}$$

When port I excited $\vec{F}_i(\theta,\varphi)$ is the pattern property of the MIMO array. The ECC value is less than 0.001 from 3.1 to 12 GHz, as seen in Fig. 20; it shows an excellent performance diversity. Equation (2) below provides the diversity gain after being calculated using ECC [28].

$$DG = 10\sqrt{1-\rho_e{}^2} \tag{2}$$

The diversity gain of the proposed UWB-MIMO antenna is depicted in Fig. 21, which is greater than the defined criterion of 9.9 at the designed frequency band.

4.2. Mean effective gain and total active reflection coefficient

Mean effective gain (MEG) is one of the essential diversity parameters. It is used to calculate the gain performance of the antenna. MEG can be calculated as given in Equation (3) [29,30].

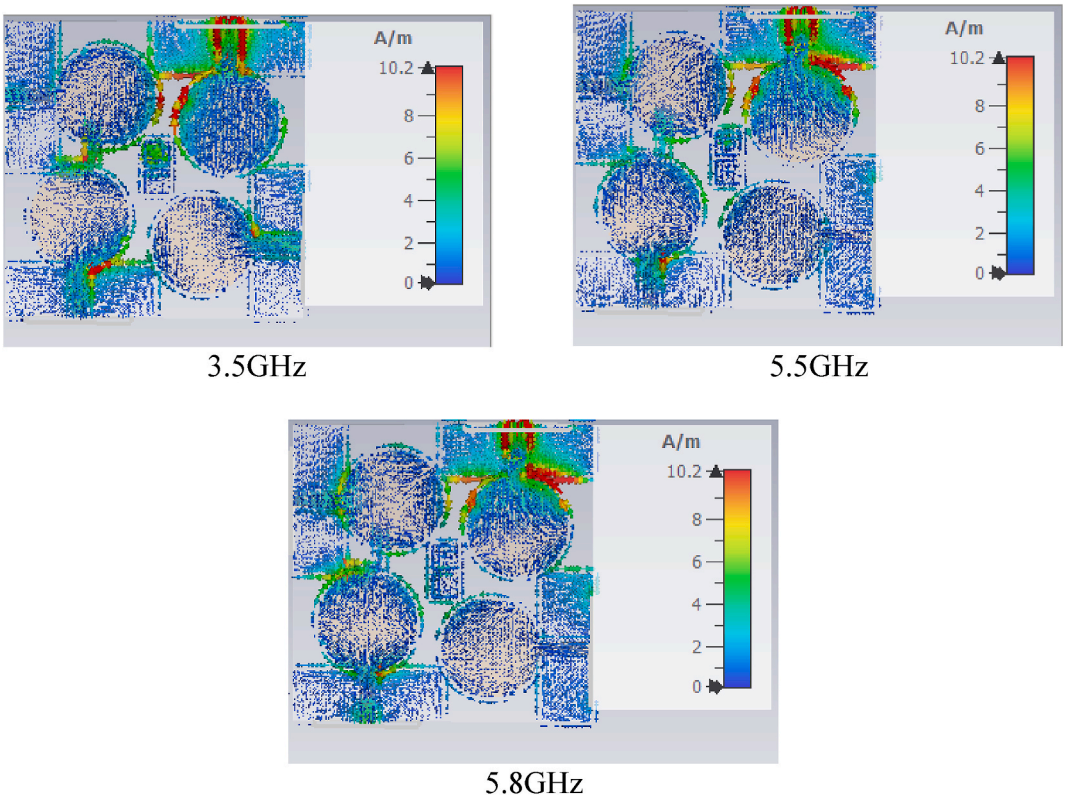

Fig. 18. Current distribution at selected frequencies of 3.5 GHz, 5.5 GHz, and 5.8 GHz when port 3 is excited.

$$\text{Mean Effective Gain} = 0.5\left[1 - \sum_{j=1}^{N}\left|S_{ij}\right|^2\right] \tag{3}$$

N is the number of antennas, and i represents the observation port. The MIMO antenna's MEG must be lower than −3 dB [31]. Fig. 22 depicts the MEG fluctuation for the proposed antenna. It can be seen from the curve that the MEG is less than −3 dB. TARC can be used to measure the signal interference between MIMO channels. It is denoted mathematically by Refs. [32,33] as presented in Equation (4):

$$\Gamma_a^t = \sqrt{\frac{\sum_{i=1}^{N}\left|b_i\right|^2}{\sum_{i=1}^{N}\left|a_i\right|^2}} \tag{4}$$

where t is denoted as total, a is active, a_i is the incident signal, and b_i is the signal that was reflected. It can be further calculated by Eq. (5):

$$TARC = \frac{\sqrt{\left|S_{11} + S_{12}e^{j\theta}\right|^2 + \left|S_{22} + S_{21}e^{j\theta}\right|^2}}{\sqrt{2}} \tag{5}$$

where θ is the phase angle between 0° and 180°. The simulated and measured TARC is depicted in Fig. 23 at three different angles 0°, 30°, and 60°, and it is observed that TARC is less than −10 dB throughout the operating frequency band.

4.3. Channel capacity loss

When assessing the effectiveness of MIMO antenna arrays, channel capacity loss is another crucial issue to consider. Mathematically it can be defined by Eqs. (6) and (7) [34, 35, 36].

$$C_{loss} = -\log_2 \det\left(\alpha^R\right) \tag{6}$$

where

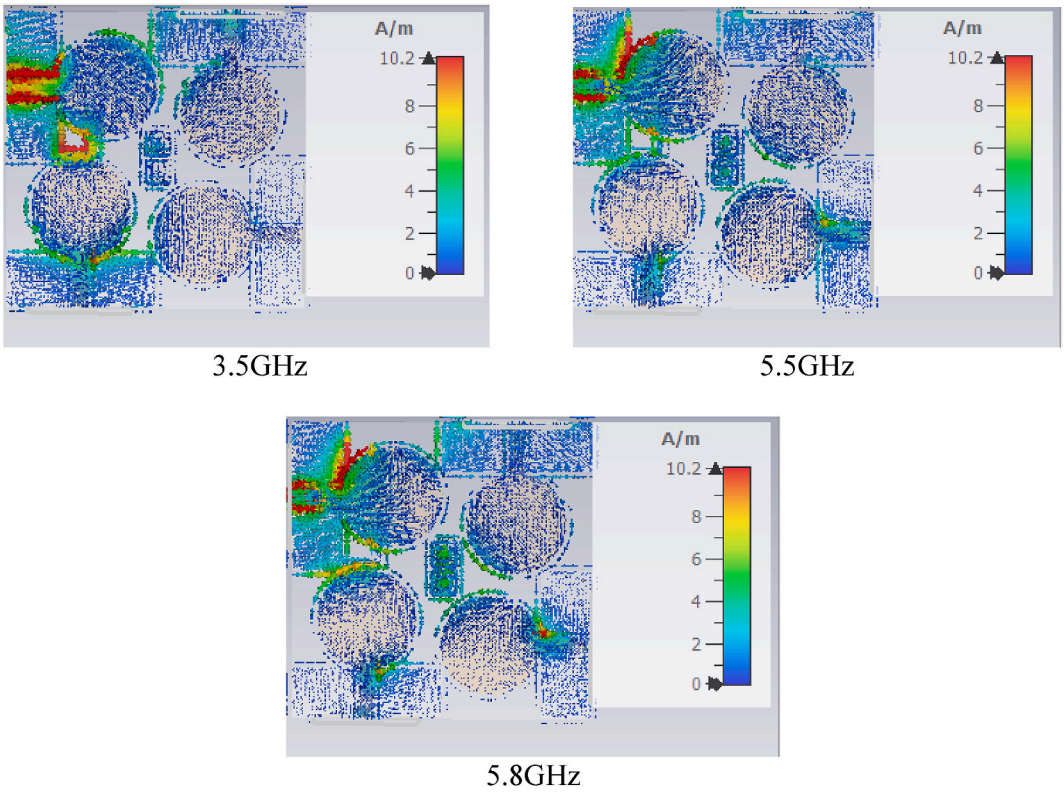

Fig. 19. Current distribution at selected frequencies of 3.5 GHz, 5.5 GHz, and 5.8 GHz when port 4 is excited.

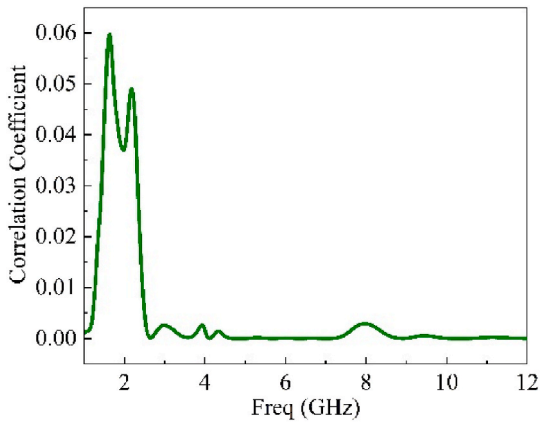

Fig. 20. ECC of UWB-MIMO antenna.

$$\alpha^R = \begin{vmatrix} x_{11} & x_{12} & x_{13} & x_{14} \\ x_{21} & x_{22} & x_{23} & x_{24} \\ x_{31} & x_{32} & x_{33} & x_{34} \\ x_{41} & x_{42} & x_{43} & x_{44} \end{vmatrix} \tag{7}$$

Fig. 24 displays the measured and simulated CCL, and it is obvious that the CCL value is < 0.1 bits/s/Hz over the whole frequency range. The minimum bit rate for channel capacity loss is 0.4 bits/s/Hz [37]. The proposed UWB-MIMO antenna's performance is compared against other designs published by other researchers, as shown in Table 4. Our proposed antenna outperforms most reported antennae in size, gain, and efficiency.

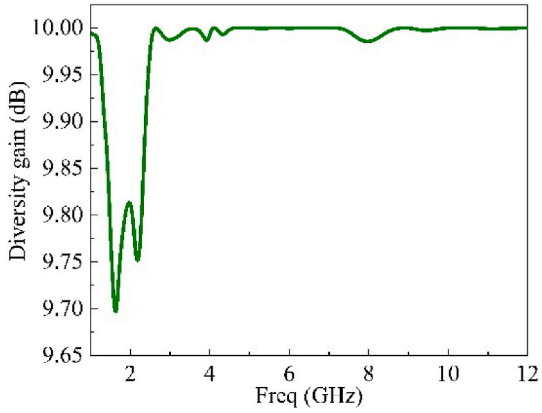

Fig. 21. Diversity gain of UWB-MIMO antenna.

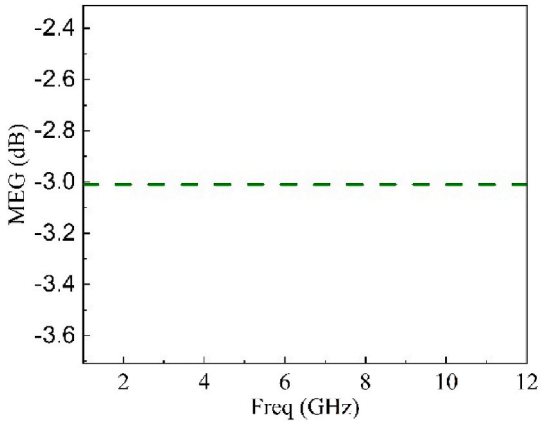

Fig. 22. MEG of UWB-MIMO antenna.

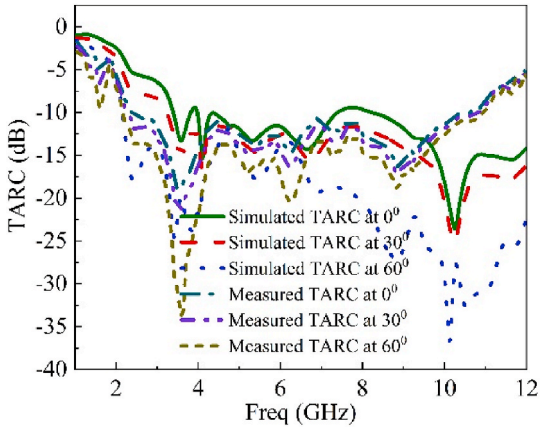

Fig. 23. Simulated and measured TARC of UWB-MIMO antenna.

5. Conclusions

This paper presents and discusses the design of a four-port cross-polarized MIMO antenna using two metamaterial unit cells. Antenna patch vertices have been enhanced with curved edges. This MIMO antenna exhibits a UWB range (3.1–12) GHz, 6.2 dBi peak gain, 87% total efficiency, and isolation of −17 dB, respectively. According to the proposed system, the ECC, TARC, DG, and MEG are

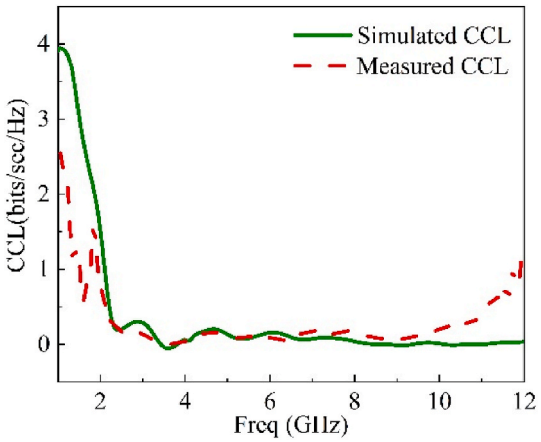

Fig. 24. Measured and simulated CCL of UWB-MIMO antenna.

Table 4
Comparison of the proposed antenna with various UWB-MIMO antennas.

Ref.	No. of Ports	Size (mm)	Isolation Technique	Spacing (mm)	Max. Gain (dBi)	Efficiency (%)	Isolation (dB)	ECC, DG	CCL, TARC
[13]	4	75.19 × 75.19 × 1.6	Neutralization ring	33	5	NG	15.9	<0.1, NG	NG, NG
[18]	4	56 × 68 × 0.2	Diamond shape slot	6	5.87	NG	15	<0.02, NG	<0.5, <−10
[19]	4	34 × 34 × 1.6	EBG structure	NG	5.5	90	15	<0.05, NG	NG, <0
[23]	4	80 × 80 × 1.6	Split ground	NG	5.8	80	25	<0.02, >9.9	<0.4, <−10
[24]	4	48 × 34 × 1.6	Neutralization lines	8	2.91	79.8	23	<0.039, >9.81	<0.29, <−10
[26]	4	74 × 74 × 1.524	Parasitic elements & slots	NG	7.68	94	34	NG, NG	NG, NG
[32]	4	36 × 35 × 1.6	DGS	NG	NG	NG	17	<0.012, >9.99	NG, <−6
[33]	4	40 × 40 × 1.524	DGS	4.25	3.5	89	15	<0.4, >9.95	<0.22, NG
[34]	4	40 × 40 × 1.6	DGS	NG	2.36	NG	25	<0.21, >9.71	<0.13, NG
Proposed design	4	30 × 30 × 1.6	MTM & DGS	9.75	6.2	87	17	<0.001, >9.9	<0.1, <−10

NG = Not Given.

0.001, <−10 dB, 9.98 dBi, and <−3 dB. The total CCL is less than 0.1 bps/Hz over the entire operational bandwidth, making the antenna a promising candidate for WLAN, WIMAX and GPRs applications. The equivalent circuit model has been presented and discussed. Future work will focus on adding more antennas for transmitting and receiving to increase throughput. Furthermore, combining the proposed method with another method can enhance the coupling effect between the MIMO elements.

Declaration of competing interest

The authors declare no conflict of competing interest.

Acknowledgments

The authors would like to acknowledge the technical and financial support provided by United Arab Emirates University.

References

[1] D. Haripriya, S. Venkatakiran, A. Gokulachandar, UWB-MIMO antenna of high isolation two elements with WLAN single band-notched behavior using roger material, Mater. Today Proc. 62 (2022) 1717–1721.
[2] T.S. Hiwa, N. Javal, G. Ghangiz Ghobadi, A novel shaped antenna for designing UWB-MIMO system in microwave communications, Int. J. Electron. Commun. 152 (2022) 1–13.

[3] K. Jayshri, D. Arpan, D. Chow-yen, Wideband four port MIMO antenna array with high isolation for future wireless systems, Int. J. Electron. Commun. 128 (2021) 1–14.
[4] N.P. Kulkarni, N.B. Bahadure, P.D. Patil, J.S. Kulkarni, Flexible interconnected four port MIMO antenna for sub 6GHz 5G and X band communications, Int. J. Electron. Commun. 152 (2022) 1–14.
[5] G. Singh, S. Kumar, B.K. Kanaujia, V.J. Pandey, Design and performance analysis of a frequency reconfigurable four-element multiple-input-multiple-output antenna, Int. J. Electron. Commun. 146 (2022) 1–12.
[6] J.A. Tirado-Mendez, H. Jordan-Aguilar, R. Flores-Leas, et al., Metamaterial split ring resonator applied as reduced size four-port antenna array for MIMO applications, Int. J. Electron. Commun. 154 (2022) 1–6.
[7] H. Ekrami, S. Jam, A compact triple-band dual-element MIMO antenna with high port-to-port isolation for wireless applications, Int. J. Electron. Commun. 96 (2018) 1–9.
[8] M. Alibakhshikenari, B.S. Virdee, C.H. See, et al., Surface wave reduction in antenna arrays using metasurface inclusion in MIMO and SAR systems, Radio Sci. 54 (1) (2019) 1067–1075.
[9] Vishal Puri, Hari Shankar Singh, Design of isolation improved MIMO antenna design using a meta-surface-based absorber for wireless applications, Optik-Int. J. Light Electr. Opt. 259 (2022) 1–11.
[10] M.N. Hassan, S. Chu, S.A. Bashir, DGS monopole antenna loaded with U-shape stub for UWB MIMO applications, Microw. Opt. Technol. Lett. 61 (2019) 2141–2149.
[11] H. Jiang, L.M. Si, G. Cheng, X. Lv, A wideband closed speed 5G MIMO antenna with mutual coupling reduction using combined decoupling networks, in: 2019 Int. Conference on Microwave and Millimeter Wave Technology (ICT), 2019, pp. 1–3.
[12] Kompella S.L. Parvathi, Sudha R. Gupta, Novel dual-band EBG structure to reduce mutual coupling of air gap-based MIMO antenna for 5G application, Int. J. Electron. Commun. 138 (2021) 1–8.
[13] A. Kayabasi, A. Toktas, E. Yigit, K. Sabanci, Triangular quad-port multi-polarized UWB MIMO antenna with enhanced isolation using neutralization ring, Int. J. Electron. Commun. 85 (2018) 47–53.
[14] K.T. Phuong, H.T. Huy, T.L. Tuan, Circularly polarized MIMO antenna utilizing parasitic elements for simultaneous improvement in isolation, bandwidth, and gain, Int. J. Electron. Commun. 135 (2021) 1–7.
[15] H.J. Adamu, H.-X. Zheng, A. Anas, S. Zhiwei, Characteristic mode analysis and design of wideband MIMO antenna consisting of metamaterial unit cell, Electronics 68 (8) (2019) 1–14.
[16] L. Shuang, W. Daigiang, Yuqing C, Ershi Li, J. Gong, A compact dual port UWB MIMO antenna with quadruple band-notched characteristics, Int. J. Electron. Commun. 136 (2021) 1–9.
[17] Sumon Modak, Taimoor Khan, A slotted UWB-MIMO antenna with quadruple band-notch characteristics using mushroom EBG structure, Int. J. Electron. Commun. 134 (2021) 1–6.
[18] D. Arpan, K. Jayshri, M.M. Kamaruzzaman, et al., Interconnected CPW fed flexible 4-port MIMO antenna for UWB, X, and Ku band applications, IEEE Access 10 (2022) 57641–57654.
[19] Z. Chen, W. Zhou, J. Hong, A miniaturized MIMO antenna with triple band-notched characteristics for UWB applications, IEEE Access 9 (2021) 63646–63656.
[20] B. Yang, S. Qu, A compact integrated Bluetooth UWB dual-band notch antenna for automotive communications, Int. J. Electron. Commun. 80 (2017) 104–113.
[21] Mousa I. Hussein, Hakam Ali, Mohamed Ouda, et al., Compact low profile planar elliptical antenna for UWB applications, in: 2016 10th European Conference on Antennas and Propagation, 2016, pp. 1–2.
[22] J. Tao, Q. Feng, Compact ultra-wideband MIMO antenna with half slot structure, IEEE Antenn. Wireless Propag. Lett. 16 (2017) 792–795.
[23] S.D.R. Vutukuri, P. Pokkunuri, T.P.M. Boddapati, U.D. Yalavarthi, Dual band-notched orthogonal 4-element MIMO antenna with isolation for UWB applications, IEEE Access 8 (2020) 145871–145880.
[24] N.T. Rakesh, S. Prabhakar, K.K. Binod, S. Kunal, Neutralization technique baseband and four-port high isolation MIMO antennas for UWB communication, Int. J. Electron. Commun. 110 (2019) 1–10.
[25] T.C. Hassan, L. Farah, A.T. Farooq, et al., Small-sized UWB-MIMO antenna with band rejection capability, IEEE Access 7 (2019) 121816–121824.
[26] F. Yanal, A. Sarosh, N. Salman, et al., Compact super wideband frequency diversity hexagonal-shaped monopole antenna with switchable rejection band, IEEE Access 10 (2022) 42321–42333.
[27] A.H. Jabire, A. Ghaffar, X.J. Li, et al., Metamaterial based design of compact UWB/MIMO monopoles antenna with characteristics mode analysis, Appl. Sci. 11 (2021) 1542.
[28] A.B. Murtala, K.A.I. Mohamad, Z. Farid, et al., A compact triband miniaturized MIMO antenna for WLAN applications, Int. J. Electron. Commun. 136 (2021) 1–15.
[29] M.D. Abu sufian, Niamat Hassan, Ameer Abbas, et al., Mutual coupling reduction of a circularly polarized MIMO antenna using parasitic elements and DGS for V2V communications, IEEE Access 10 (2022) 56388–56400.
[30] P. Prabhu, S. Malarvizhi, Design and packaging of polarization diversity 3D-UWB MIMO antenna with dual-band notch characteristics for vehicular communication applications, Int. J. Electron. Commun. 138 (2021) 1–10.
[31] M. Asutosh, R.B. Bikash, Investigation of 2-port UWB-MIMO diversity antenna design using characteristic mode analysis, Int. J. Electron. Commun. 124 (2020) 1–9.
[32] P. Pannu, D.K. Sharma, Miniaturized four port UWB-MIMO antenna with tri-notched band characteristics, Microw. Opt. Technol. Lett. 63 (2021) 1489–1498.
[33] A.K. Aqeel, A.N. Syed, S.K. Muhammad, I. Bilal, Quad-port miniaturized MIMO antenna for UWB 11GHz and 13GHz frequency bands, Int. J. Electron. Commun. 131 (2021) 1–7.
[34] A. Iqbal, A. Smida, A.J. Alazani, et al., Wideband circularly polarized MIMO antenna for high data wearable biotelemetric devices, IEEE Access 8 (2020) 17935–19944.
[35] I. Elegant, A. Iqbal, C. Zebiri, et al., Low profile and closely spaced four-element MIMO antenna for wireless body area networks, Electronics 9 (2020) 258.
[36] M.A. Abdalla, A.A. Ibrahim, Design and performance evaluation of Metamaterial inspired MIMO antennas for wireless applications, Wireless Pers. Commun. 95 (2017) 1001–1017.
[37] Arashprit K. Sohi, K. Amanpreet, Triple band stop characteristics from an aperture coupled modified Pythagoras tree fractal-based UWB-MIMO antenna integrated with complementary hexagonal spiral defected ground structure, Int. J. Electron. Commun. 137 (2021) 1–16.